

2D correlations in the van der Waals ferromagnet CrBr₃ using high frequency electron spin resonance spectroscopy

Cite as: J. Appl. Phys. 129, 233902 (2021); doi: 10.1063/5.0051651

Submitted: 26 March 2021 · Accepted: 31 May 2021 ·

Published Online: 17 June 2021



View Online



Export Citation



CrossMark

C. L. Saiz,¹ J. A. Delgado,¹ J. van Tol,² T. Tartaglia,³ F. Tafti,³ and S. R. Singamaneni^{1,a}

AFFILIATIONS

¹ Department of Physics, The University of Texas at El Paso, El Paso, Texas 79968, USA

² National High Magnetic Field Laboratory, Florida State University, Tallahassee, Florida 32310, USA

³ Department of Physics, Boston College, Chestnut Hill, Massachusetts 02467, USA

^aAuthor to whom correspondence should be addressed: srao@utep.edu

ABSTRACT

Broadening the knowledge and understanding on the magnetic correlations in van der Waals layered magnets is critical in realizing their potential next-generation magneto-electronic applications. In this study, we employ high-frequency ($v = 240$ GHz) electron spin resonance (ESR) spectroscopy on plate-like quasi two-dimensional (2D) CrBr₃ to gain insight into the magnetic interactions as a function of temperature (4–200 K) and the angle of rotation. We find that the temperature dependence of the ESR linewidth is well described by the Ginzburg–Landau critical model, indicative of the presence of 2D correlations. Furthermore, our findings show that the resonance field follows a $(3 \cos^2 \theta - 1)$ -like angular dependence, while the linewidth follows a $(3 \cos^2 \theta - 1)^2$ -like angular dependence, a behavior indicative of 2D correlations that are likely due to the interaction of the external magnetic field applied during the ESR experiment. This study demonstrates the significance of employing spin sensitive techniques such as ESR to better understand the magnetic correlations in similar van der Waals magnets.

Published under an exclusive license by AIP Publishing. <https://doi.org/10.1063/5.0051651>

I. INTRODUCTION

Among various van der Waals (vdW) magnets, CrX₃ (where X = Cl, Br, I) is a family of compounds that has gained considerable attention due to their cleavable nature and persistent magnetic properties even at the atomic limit.^{1–5} Of these, CrBr₃ is a soft out-of-plane ferromagnetic (FM) insulator with a Curie temperature (T_C) of about 33 K^{5,6} and has been reported to show spontaneous magnetization down to the monolayer.⁷ It is an interesting platform to study magnetic interactions as atomically thin CrBr₃ has been shown to exhibit ferromagnetic interlayer coupling,⁸ while recent spin-polarized scanning tunneling microscopy and spectroscopy studies have confirmed this coupling to be either ferromagnetic (FM) or antiferromagnetic (AFM) in the bilayer depending on the stacking order.¹ Basic magnetic properties of this title compound have been reported earlier^{9,10} with magnetism arising from the Cr³⁺ ion ($S = 3/2$, spin-only contribution) and the easy axis of magnetization along the c axis.

Electron paramagnetic/spin resonance (EPR/ESR) spectroscopy is an ideal tool to study the magnetic interactions and magnetic anisotropy in vdW magnetic materials.^{11–15} For instance, through the use of high-frequency ($v = 240$ GHz) ESR spectroscopy, Lee *et al.* have reported on the fundamental spin interactions that cause the magnetic anisotropy in CrI₃.¹¹ In another study, ESR spectroscopy was carried out at various frequencies in the presence of a high magnetic field in order to investigate the magnetic anisotropy in another vdW magnet, Cr₂Ge₂Te₆.¹² In another recent work, Zeisner *et al.* again used high-field ESR spectroscopy over a range of frequencies to prove the existence of ferromagnetic short-range correlations above the magnetic phase transition and established the intrinsically two-dimensional (2D) nature of the magnetism in CrCl₃.¹³ Of significant relevance, through numerous ESR studies on the spin dynamics of the 2D triangular Cr-antiferromagnetic frustrated lattices ACrO₂ (where A = Li, Na, Cu, Ag), Hemmida *et al.* have determined that there exists a

dominant role of magnetic vortices for the spin relaxation in ACrO_2 and call for further investigations on similar compounds.^{16–19} Additionally, our group has employed light-induced ESR spectroscopy to study photoexcited magnetic interactions in CrI_3 and CrCl_3 .¹⁵

While numerous ESR works have been carried out on two compounds of the CrX_3 family (CrI_3 and CrCl_3), to our knowledge, there has been only a few ESR works reported on CrBr_3 in the last 50 years.^{20,21} However, the temperature dependence of the ESR linewidth as well as the angular dependence of the ESR resonance field and linewidth have not been discussed in detail. The temperature and angular dependences of the ESR spectral parameters such as signal width and resonance field provide fingerprint-like signatures of magnetic phase transitions as well as information on microscopic magnetic interactions, which appears to be missing from the literature. Since the magnetic resonance properties of bulk CrBr_3 serve as a basis for the understanding of magnetic phenomena in reduced dimensions, e.g., in few- or monolayer samples of CrBr_3 , a profound understanding of magnetic correlations in CrBr_3 is needed, especially considering that magnetic mono/few-layer CrBr_3 have now become accessible.⁷ Here, through the use of high-frequency ($v = 240 \text{ GHz}$) ESR spectroscopy, we show that the temperature dependence of the ESR linewidth, reflective of spin dynamics, follows the Ginzburg–Landau critical model satisfactorily, giving critical exponents indicative of two-dimensionality in bulk CrBr_3 . In addition, we find that the Berezinskii–Kosterlitz–Thouless (BKT) transition model is not applicable due to the absence of magnetic phase separation. Furthermore, we find that the angular dependence of the linewidth and resonance field from CrBr_3 points toward 2D correlations, though the precise origin is yet to be resolved.

II. EXPERIMENTAL DETAILS

CrBr_3 single crystals of dimension $1 \times 1 \text{ mm}^2$ were grown by the chemical vapor transport method as previously reported by some of us.^{22,23} High-frequency ESR measurements were conducted at the National High Magnetic Field Laboratory located at Florida State University using the quasi-optical spectrometer developed on-site. This system uses a superheterodyne spectrometer, employing a quasi-optical submillimeter bridge that operates in reflection mode without cavity using a sweepable 17 T superconducting magnet.¹⁴ In order to conduct ESR measurements as a function of angle θ (degrees) at $T = 200$ and 4 K, the sample was loaded into the instrument while attached to a sample rotator, allowing the plate-like sample to be rotated along the c axis during ESR measurements. The CrBr_3 unit cell and atomic structure of the monolayer are shown in Fig. 1. The sample was cooled from room temperature down to 200 K before a magnetic field was applied in order to ensure that the vacuum grease used to attach the sample to the rotator is solidified. ESR measurements were performed at $v = 240 \text{ GHz}$ as a function of θ at both $T = 200 \text{ K}$ (paramagnetic phase) and 4 K (ferromagnetic phase) while the plate-like sample was rotated. Measurements were also conducted while the sample was held at a fixed angle of $\theta = 70^\circ$, due to an apparent field minimum at that angle, at the temperature range of $T = 4\text{--}200 \text{ K}$ (as shown in Fig. 2). Magnetic susceptibility measurements were

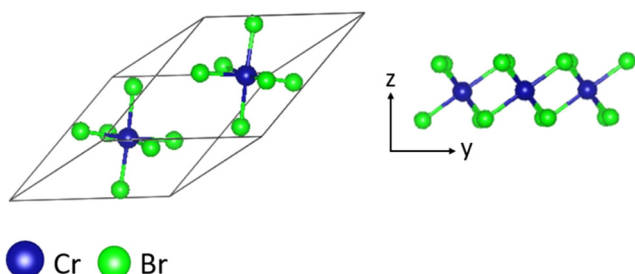


FIG. 1. Trigonal CrBr_3 unit cell and a side view of the monolayer atomic structure.

performed by employing a Quantum Design MPMS-3 SQUID magnetometer using a DC method.^{22,23}

III. RESULTS AND DISCUSSION

Figure 2 shows the 240 GHz ESR spectra collected at the fixed angle of $\theta = 70^\circ$ over the temperature range of 4–200 K in order to gain insight into the behavior of the linewidth (full width at half maximum, ΔH) and resonance field.

It is observed that the single paramagnetic signal of Lorentzian line shape at 200 K with $g = 2.016$ begins to split into multiple signals as the sample is cooled from 4–200 K. The temperature at which the single signal becomes multiple is in the vicinity of $T_C = 33 \text{ K}$. Below $T = 32 \text{ K}$ down to 4 K, multiple signals arise, and the paramagnetic signal broadens. Due to the high sensitivity of ESR spectroscopy, compared to conventional magnetometers, this technique is able to pick up ferromagnetic correlations even at $T \gg T_C$ as reflected through the appearance of multiple signals at $T > 32 \text{ K}$, consistent with previous reports.^{11–13} Numerous ESR signals, as seen in

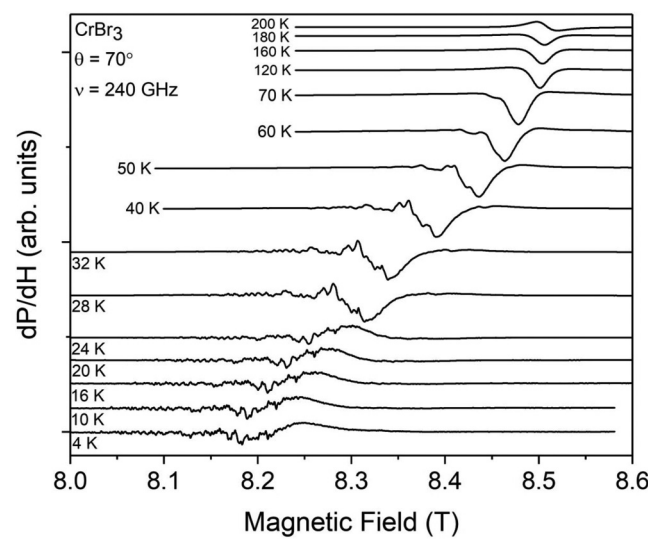


FIG. 2. ESR signals as a function of temperature at a single fixed angle.

this experiment, are typically observed in ferromagnetic compounds due to magnetocrystalline anisotropy, magnetic inhomogeneity, and magnetic phase separation.^{24–29} It is also worth noting that the spectroscopic *g*-value is seen to increase at a somewhat exponential rate as the temperature is lowered from $T = 4\text{--}200\text{ K}$ (not shown). At $T = 200\text{ K}$, $g = 2.016$ and at $T = 4\text{ K}$, $g = 2.082$. This *g*-value is within close proximity to $g = 2$ and is indicative of a quenched orbital moment that is typically seen in the Cr³⁺ ion.^{16,17} This exponential behavior begins at $T = 40\text{ K}$, within close proximity to T_C , suggesting that this sharp change in *g*-value can be attributed to the creation of internal magnetic correlations as the temperature approaches the magnetic phase transition from above.

A. Ginzburg-Landau critical model and BKT transition

The ESR spectral parameters were extracted using a Lorentzian (curve in red) fit at each temperature in the paramagnetic phase (40–200 K), some of which are shown in Fig. 3. It should be noted that the narrow ESR signals modulated by a broader signal for the spectra measured at and below the magnetic phase transition were not fitted due to their apparent complexity. We first discuss the temperature dependence of the ESR linewidth as plotted in Fig. 4. Figure 4 shows the variation of linewidth as a function of temperature represented by solid squares, where the superimposed red curve is the computer-generated fit resulting from the Ginzburg-Landau critical model. The critical model states that

$$\Delta H(T) = \frac{Q}{\left(\frac{T}{T_C} - 1\right)^p} + mT + \Delta H_0, \quad (1)$$

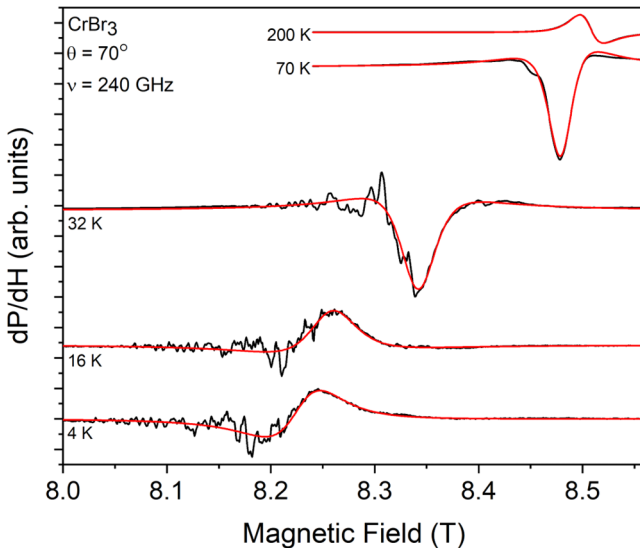


FIG. 3. Computer-generated fits employing a Lorentzian line shape over a range of temperatures represented by the smooth red curve. The black curve is the collected ESR spectra.

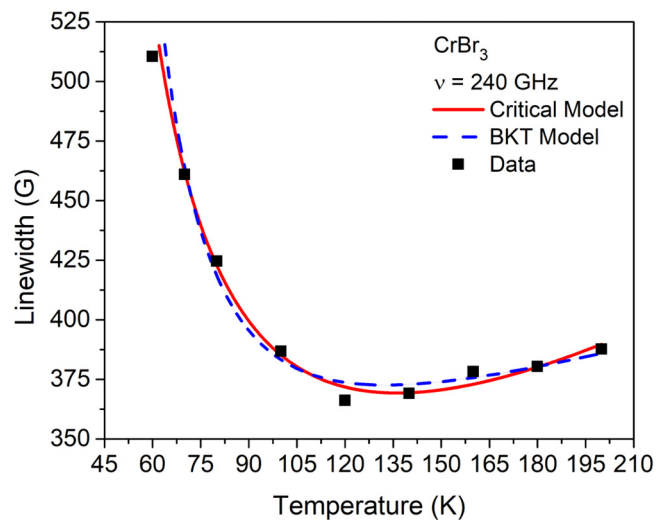


FIG. 4. Temperature dependence of the ESR linewidth at the fixed angle $\theta = 70^\circ$; fitted to the Ginzburg-Landau critical model (solid red line) and the Berezinskii-Kosterlitz-Thouless model (dashed blue line).

in which Q is an arbitrary constant of proportionality, T_C is the Curie temperature, and p is a critical exponent, which is dependent on the spatial and spin degrees of freedom and can give a clear description of the dimensionality. The linear term m and a temperature independent term ΔH are added to describe the physics far away from the magnetic phase transition.^{30,31} Figure 4 also shows the variation of linewidth as a function of temperature along with the fit generated using the BKT model, a phase transition that takes place at finite temperatures previously understood to be unique to the 2D XY model, a limiting case of the 2D Heisenberg model.⁵ A transition of this type is not usually observed in condensed matter systems due to inherent interlayer coupling, which inhibits the BKT transition due to long-range order,³⁰ a property that 2D Heisenberg magnets lack at finite temperatures.³ The BKT transition, which is typically found in 2D systems approximated by the XY model, asserts

$$\Delta H(T) = \Delta H_\infty \exp\left[\frac{3b}{\sqrt{\left(\frac{T}{T_{BKT}} - 1\right)}}\right] + mT + \Delta H_0. \quad (2)$$

In our experiment, b has been set to $\pi/2$ for a square lattice in consistency with previous reports, although it has been shown to remain valid at any value.³² Figure 4 illustrates that our obtained ESR data are described very nicely by (1) and (2) in the region well above the magnetic phase transition (see Table I for extracted fit parameters), with the extrapolated critical exponent $p = 0.9$. This is very close to the reported value of $p = 0.5\text{--}0.7$, which has been reported in most of the previously investigated layer-type antiferromagnets studied by Benner and Boucher.³³ Similar values of

TABLE I. Values of fit parameters and goodness of fit obtained from the Ginzburg-Landau critical model and BKT model.

Critical model	BKT model
Exponent from fit	Exponent from fit
Q (T)	294.1
p	0.9043
T_C (K)	32
m (T/K)	0.8759
H (T)	117.5
R^2	0.9903
H_{BKT} (K)	13.74
b	$\pi/2$
H_∞ (T)	27.64
m (T/K)	0.8641
R^2	0.9906

$p = 0.78$ and 0.85 have also been reported in HCrO_2 and NaCrO_2 , respectively, and are suggestive of antiferromagnetic fluctuations.¹⁶ A similar BKT-like transition has been observed in the Cr^{3+} -doped three-dimensional (3D) magnets such as $\text{Bi}_{0.5}\text{Sr}_{0.5}\text{Mn}_{0.9}\text{Cr}_{0.1}\text{O}_3$ by Ashoka *et al.*^{30,34} Through the temperature dependence of the ESR linewidth, the authors employed the BKT model to satisfactorily describe their experimental findings. The authors explained this observation in terms of an effective 2D XY easy plane anisotropy induced by the magnetic field applied in the ESR experiment that presumably induces an interaction between the long-range spin vortices and spin clusters that may have been formed during magnetic phase segregation.³⁰ In a separate study, these authors tested the hypothesis that the applied EPR field is responsible for the onset of BKT-like behavior in $\text{BaNi}_2\text{V}_2\text{O}_8$ and have shown that a higher applied field allows for a higher temperature onset of the threshold anisotropy required for BKT behavior, which will manifest as a higher T_{BKT} .³⁴ This behavior is evidenced in another work, where Seehra and Gupta find that the ESR linewidth in CrBr_3 behaves differently when the frequency is increased from 9.1 to 24 GHz.²¹ As the applied field increases, the thermal behavior of the linewidth and correlation length around T_C begins to vary, where the spectroscopic linewidth broadens from $\Delta H \sim 55$ Oe at $v = 9.1$ GHz to $\Delta H \sim 65$ Oe at $v = 24$ GHz. This is in good agreement with our data at $v = 240$ GHz, where the linewidth is calculated to be $\Delta H = 670$ Oe at $T = 32$ K (not shown).

B. Angular dependence of the resonance field

We now focus on the angular dependence of the ESR resonance field and linewidth. In Fig. 5(a), we have plotted the resonance field (solid squares, left y axis) as well as the g-value (hollow inverted triangles, right y axis) as a function of angle collected at $T = 200$ K. The g-values were interpolated with a spline function, shown as dashed curve. The angular dependence of the resonance field is fitted with the model,

$$H_{res}(\theta) = F(3\cos^2\theta - 1) + G. \quad (3)$$

The observed $(3\cos^2\theta - 1)$ -like behavior of the resonance field is a characteristic behavior of 2D magnetic systems^{35,36} and has earlier been observed in K_2MnF_3 , K_2CuF_3 , and CrCl_3 , which has been experimentally shown to exhibit 2D Heisenberg behavior

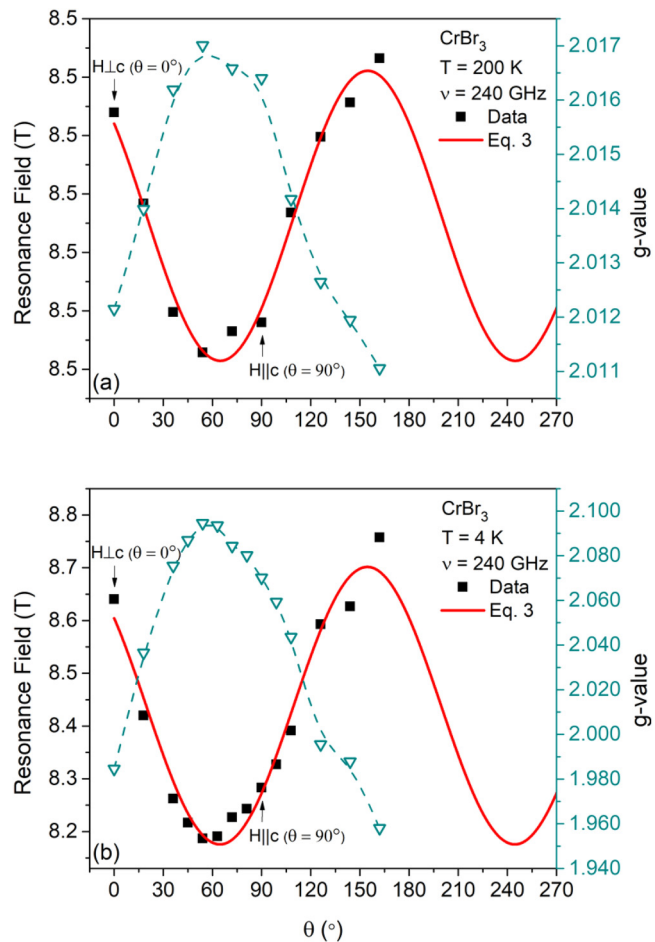


FIG. 5. Angular dependence of the resonance field at (a) 200 K and (b) 4 K fitted with a modified form of (3) to take into account a phase shift: $H_{res}(\theta) = F[3\cos^2(\theta - \phi) - 1] + G$. Here, the cyan data points show the calculated g-values with a B-spline to guide the eye and illustrate the inverse relationship between resonance field and g-value.

and is reported to have correlations suggestive of a weak XY model.^{35,37,38} The curve connecting the resonance field values results from the fit using (3). An identical trend is observed for the angular dependence of resonance field and g-value when the measurement is conducted at $T = 4$ K, as plotted in Fig. 5(b). This marked angular dependence of the resonance field at both temperatures has been described as the noncubic distribution of the dipoles within the 2D lattice where the resulting net dipolar field shifts the resonance field according to (3).³⁵

C. Angular dependence of the linewidth

Equation (4) accurately and adequately describes the dependence of the linewidth on θ , both in the ferromagnetic and

paramagnetic phases as seen in Fig. 6,

$$\Delta H(\theta) = A(3 \cos^2 \theta - 1)^2 + B. \quad (4)$$

The nearly “W”-shaped angular dependence of the linewidth observed here is unique to low-dimensional magnets and has been previously reported in MnPS₃, a compound that has been shown to have 2D characteristics,³⁹ as well as other 2D magnetic systems such as the 2D antiferromagnet K₂MnF₄³³ and the in-plane 2D Heisenberg antiferromagnet CrCl₃.³⁵ The unique shape of this curve with a maximum near lower angles and a shallow minimum near $\theta = 55^\circ$, or the “magic” angle, has been observed in other systems and is a known feature of low-dimensional systems.³³

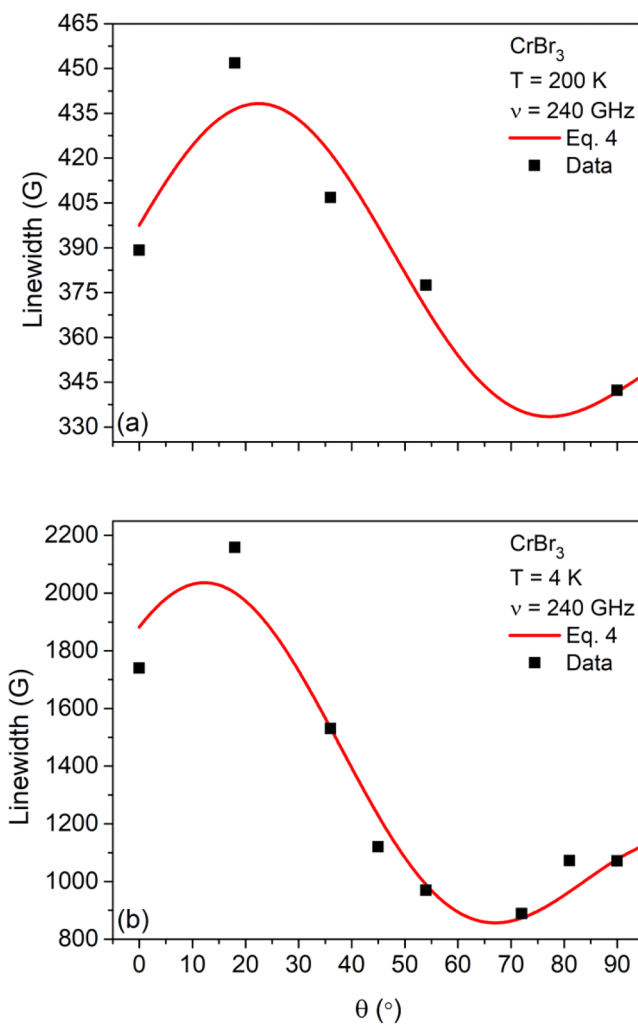


FIG. 6. Angular dependence of the linewidth at (a) 200 K and (b) 4 K fitted with a modified form of (4) to take into account a phase shift: $\Delta H(\theta) = A[3\cos^2(\theta - \phi) - 1]^2 + B$.

Similar to the model described by (3), this $(3 \cos^2 \theta - 1)^2$ -like behavior is also characteristic of 2D magnetic systems.³⁵

Bulk CrBr₃ has traditionally been known as a single phase ferromagnet.^{4,5,9,10} Quite interestingly, in a recent report using Raman spectroscopy mapping, Li *et al.*³⁸ revealed a novel mixed state of layered antiferromagnetism and ferromagnetism in 3D CrI₃ bulk crystals where the layered antiferromagnetism survives in the surface layers and the ferromagnetism appears in deeper bulk layers. Due to the structural similarities between CrI₃ and the title compound, one may expect that the latter will also exhibit magnetic phase separation. Therefore, in trying to understand the origin of 2D correlations, temperature dependent magnetization measurements were conducted upon zero-field- and field-cooled (ZFC and FC) conditions from $T = 2$ –300 K. For FC measurements, a magnetic field of $H = 0.01$ T was applied along the *c* axis (easy axis) while cooling the sample. As shown in Fig. 7, a clear bifurcation between ZFC and FC traces is observed below T_C (see supplementary information in Ref. 22). This single-crystalline CrBr₃ sample is well characterized and has been used in previous studies^{22,23} and is, therefore, expected to contain minimal crystal defects and crystal grains, suggesting that this splitting is an indicator of a possible competing minute magnetic phase present along with the dominant ferromagnetic phase. Similar splitting between the ZFC and FC curves has been reported previously in a number of low-dimensional magnets such as CeCrO₃, Pr_{0.5}Sr_{0.5}MnO₃, and the nanoscale charge ordered (CO) manganites RE_{1-x}AE_xMnO₃ (RE = Nd, Pr; AE = Ca; x = 0.5).^{24,40,41} However, as discussed below, we did not observe strong evidence of possible magnetic phase separation that may warrant the applicability of the BKT model in CrBr₃. First, in analyzing the molar magnetic susceptibility χ_{mol} we

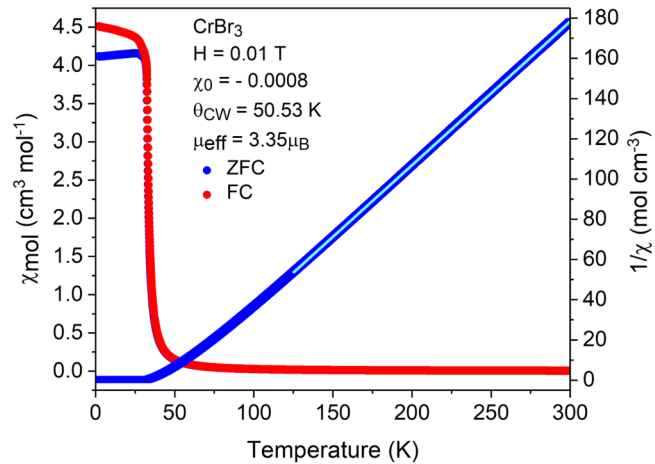


FIG. 7. Temperature dependence of magnetic susceptibility under zero-field- and field-cooled conditions show a pronounced bifurcation between ZFC (blue) and FC (red) curves (left y axis). Temperature dependence of the inverse susceptibility (blue curve, right y axis) is fitted with the CW expression (cyan line) (see supplementary material in Ref. 22). Adapted from Abramchuk *et al.*, Adv. Mater. **30**, 1801325 (2018). Copyright 2018 Author(s), licensed under a Creative Commons Attribution (CC BY) license.

have calculated a Curie–Weiss (CW) temperature of $\theta_{CW} = 50.53$ K by fitting with the CW expression $\chi - \chi_0 = C/(T - \theta_{CW})$, where C is the CW constant and χ_0 is a small background. While the frustration index²³ $f = \theta_{CW}/T_C$ is finite (>1), its magnitude is relatively smaller. Second, to our knowledge, one report⁴² appeared in the literature where the authors infer the indications of BKT behavior through the temperature dependence of susceptibility collected when the ideal 2D frustrated magnet TmMgGaO₄ is cooled under various magnetic field strengths. The authors observed that the susceptibility increases as the magnetic field decreases below $T < 2$ K (upper BKT transition), suggesting the onset of peculiar magnetic correlations. We did not see this behavior in our preliminary susceptibility measurements (Fig. 7) on CrBr₃, in which the susceptibility increases as the cooling field increases. That might suggest that the BKT phase does not exist in CrBr₃. Therefore, we rule out the possible presence of the BKT phase/correlations in CrBr₃. However, additional work is required to further the understanding.

IV. CONCLUSION

We have conducted high-frequency ESR spectroscopy on quasi-2D CrBr₃ as a function of temperature from $T = 4$ –200 K and as a function of angle from $\theta = 0^\circ$ to 162° to gain insight into the effects of temperature and the angular dependence of the linewidth and resonance field on magnetic correlations. We find that the Ginzburg–Landau critical model adequately describes the temperature dependence of the ESR linewidth, indicative of the presence of 2D correlations. Furthermore, this work shows that the resonance field follows a $(3\cos^2\theta - 1)$ -like angular dependence, while the linewidth follows a $(3\cos^2\theta - 1)^2$ -like angular dependence. This suggests that the quasi-2D ferromagnet, which has been described as an Ising or Heisenberg ferromagnet, could present 2D magnetic correlations. With these findings, we have illustrated the importance of employing high sensitivity spectroscopy via ESR in broadening the knowledge on magnetic correlations in low-dimensional magnets. Additional work is in progress to better understand the origin of magnetic correlations that can be likely extended to other layered vdW magnets.

ACKNOWLEDGMENTS

C.L.S., J.A.D., and S.R.S. acknowledge support from the UTEP start-up grant. T.T. and F.T. acknowledge support from the NSF-DMR (Grant No. 1708929). A portion of this work was performed at the National High Magnetic Field Laboratory, which is supported by the National Science Foundation under Cooperative Agreement No. DMR-1644779 and the State of Florida. The authors thank Professor S. V. Bhat at the Indian Institute of Science for insightful discussion during the preparation of this manuscript. SRS acknowledges support from the NSF-DMR (Award No. 2105109).

DATA AVAILABILITY

The data that support the findings of this study are available from the corresponding author upon reasonable request.

REFERENCES

- ¹W. Chen, Z. Sun, Z. Wang, L. Gu, X. Xu, S. Wu, and C. Gao, *Science* **366**(6468), 983–987 (2019).
- ²B. Huang, G. Clark, E. Navarro-Moratalla, D. R. Klein, R. Cheng, K. L. Seyler, D. Zhong, E. Schmidgall, M. A. McGuire, D. H. Cobden, W. Yao, D. Xiao, P. Jarillo-Herrero, and X. Xu, *Nature* **546**, 270–273 (2017).
- ³N. D. Mermin and H. Wagner, *Phys. Rev. Lett.* **17**, 1133 (1966).
- ⁴L. Capriotti, A. Cuccoli, A. Fubini, V. Tognetti, and R. Vaia, in *Fundamental Problems of Mesoscopic Physics*, NATO Science Series II: Mathematics, Physics and Chemistry Vol. 154 (Springer, 2004), pp. 203–216.
- ⁵H. Wang, V. Eyert, and U. Schwingenschlogl, *J. Phys.: Condens. Matter* **23**, 116003 (2011).
- ⁶X. Yu, X. Zhang, Q. Shi, S. Tian, H. Lei, K. Xu, and H. Hosono, *Front. Phys.* **14**, 43501 (2019).
- ⁷Z. Zhang, J. Shang, C. Jiang, A. Rasmussen, W. Gao, and T. Yu, *Nano Lett.* **19**(5), 3138–3142 (2019).
- ⁸D. Ghazaryan, M. T. Greenaway, Z. Wang, V. H. Guarachico-Moreira, I. J. Vera-Marun, J. Yin, Y. Liao, S. V. Morozov, O. Kristanovski, A. I. Lichtenstein, M. I. Katsnelson, F. Withers, A. Mishchenko, L. Eaves, A. K. Geim, K. S. Novoselov, and A. Misra, *Nat. Electron.* **1**, 344–349 (2018).
- ⁹H. H. Kim, B. Yang, S. Li, S. Jiang, C. Jin, Z. Tao, G. Nichols, F. Sfigakis, S. Zhong, C. Li, S. Tian, D. G. Cory, G.-X. Miao, J. Shan, K. F. Mak, H. Lei, K. Sun, L. Zhao, and A. W. Tsien, *Proc. Natl. Acad. Sci. U.S.A.* **116**(23), 11131–11136 (2019).
- ¹⁰L. Webster and J.-A. Yan, *Phys. Rev. B* **98**, 144411 (2018).
- ¹¹I. Lee, F. G. Utermohlen, D. Weber, K. Hwang, C. Zhang, J. van Tol, J. E. Goldberger, N. Trivedi, and P. C. Hammel, *Phys. Rev. Lett.* **124**, 017201 (2020).
- ¹²J. Zeisner, A. Alfonsov, S. Selter, S. Aswartham, M. P. Ghimire, M. Richter, J. van den Brink, B. Büchner, and V. Kataev, *Phys. Rev. B* **99**, 165109 (2019).
- ¹³J. Zeisner, K. Mehlawat, A. Alfonsov, M. Roslova, T. Doert, A. Isaeva, B. Büchner, and V. Kataev, *Phys. Rev. Mater.* **4**, 064406 (2020).
- ¹⁴C. L. Saiz, M. A. McGuire, S. R. J. Hennadige, J. van Tol, and S. R. Singamaneni, *MRS Adv.* **4**(40), 2169–2175 (2019).
- ¹⁵S. R. Singamaneni, L. M. Martinez, J. Niklas, O. G. Poluektov, R. Yadav, M. Pizzochero, O. V. Yazyev, and M. A. McGuire, *Appl. Phys. Lett.* **117**, 082406 (2020).
- ¹⁶M. Hemmida, H.-A. Krug von Nidda, N. Büttgen, A. Loidl, L. K. Alexander, R. Nath, A. V. Mahajan, R. F. Berger, R. J. Cava, Y. Singh, and D. C. Johnston, *Phys. Rev. B* **80**, 054406 (2009).
- ¹⁷M. Hemmida, H.-A. Krug von Nidda, and A. Loidl, *J. Phys. Soc. Jpn.* **80**, 053707 (2011).
- ¹⁸M. Hemmida, H.-A. Krug von Nidda, and A. Loidl, *J. Phys.: Conf. Ser.* **200**, 022016 (2010).
- ¹⁹M. Hemmida, H.-A. Krug von Nidda, V. Tsurkan, and A. Loidl, *Phys. Rev. B* **95**, 224101 (2017).
- ²⁰J. F. Dillon, *J. Appl. Phys.* **33**, 1191 (1962).
- ²¹M. S. Seehra and R. P. Gupta, *Phys. Rev. B* **9**, 197 (1974).
- ²²M. Abramchuk, S. Jaszewski, K. R. Metz, G. B. Osterhoudt, Y. Wang, K. S. Burch, and F. Tafti, *Adv. Mater.* **30**, 1801325 (2018).
- ²³T. A. Tartaglia, J. N. Tang, J. L. Lado, F. Bahrami, M. Abramchuk, G. T. McCandless, M. C. Doyle, K. S. Burch, Y. Ran, J. Y. Chan, and F. Tafti, *Sci. Adv.* **6**(30), eabb9379 (2020).
- ²⁴S. S. Rao and S. V. Bhat, *J. Phys. D: Appl. Phys.* **42**, 075004 (2009).
- ²⁵S. S. Rao, B. Padmanabhan, S. Elizabeth, H. L. Bhat, and S. V. Bhat, *J. Phys. D: Appl. Phys.* **41**, 155011 (2008).
- ²⁶A. I. Shames, E. Rozenberg, G. Gorodetsky, A. A. Arsenov, D. A. Shulyatev, Y. M. Mukovskii, A. Gedanken, and G. Pang, *J. Appl. Phys.* **91**, 7929 (2002).
- ²⁷V. Likodimos and M. Pissas, *Phys. Rev. B* **73**, 214417 (2006).
- ²⁸J. P. Joshi and S. V. Bhat, *J. Magn. Res.* **168**, 284 (2004).
- ²⁹E. Rozenberg, A. I. Shames, M. Auslender, G. Jung, I. Felner, J. Sinha, S. S. Banerjee, D. Mogilyansky, E. Sominski, A. Gedanken, Y. M. Mukovskii, and G. Gorodetsky, *Phys. Rev. B* **76**, 214429 (2007).

- ³⁰A. Ashoka, K. S. Bhagyashree, and S. V. Bhat, *Phys. Rev. B* **102**, 024429 (2020).
- ³¹M. Heinrich, H.-A. Krug von Nidda, A. Loidl, N. Rogado, and R. J. Cava, *Phys. Rev. Lett.* **91**(13), 137601 (2003).
- ³²J. M. Kosterlitz and D. J. Thouless, *J. Phys. C: Solid State Phys.* **6**, 1181 (1973).
- ³³H. Benner and J. P. Boucher, in *Magnetic Properties of Layered Transition Metal Compounds* (Kluwer, 1990), pp. 323–378.
- ³⁴A. Ashoka, K. S. Bhagyashree, and S. V. Bhat, *MRS Adv.* **5**, 2251–2260 (2020).
- ³⁵S. Chehab, J. Amiell, P. Biensan, and S. Flandrois, *Physica B* **173**, 211–216 (1991).
- ³⁶P. M. Richards and M. B. Salamon, *Phys. Rev. B* **9**, 32 (1974).
- ³⁷G. T. Lin, X. Luo, F. C. Chen, J. Yan, J. J. Gao, Y. Sun, W. Tong, P. Tong, W. J. Lu, Z. G. Sheng, W. H. Song, X. B. Zhu, and Y. P. Sun, *Appl. Phys. Lett.* **112**, 072405 (2018).
- ³⁸S. Li, Z. Ye, X. Luo, G. Ye, H. H. Kim, B. Yang, S. Tian, C. Li, H. Lei, A. W. Tsien, K. Sun, R. He, and L. Zhao, *Phys. Rev. X* **10**, 011075 (2020).
- ³⁹K. Okuda, K. Kurosawa, S. Saito, M. Honda, Z. Yu, and M. Date, *J. Phys. Soc. Jpn.* **55**, 4456–4463 (1986).
- ⁴⁰Y. Cao, S. Cao, W. Ren, Z. Feng, S. Yuan, B. Kang, B. Lu, and J. Zhang, *Appl. Phys. Lett.* **104**, 232405 (2014).
- ⁴¹S. S. Rao and S. V. Bhat, *J. Phys.: Condens. Matter* **21**, 196005 (2009).
- ⁴²Z. Hu, Z. Ma, Y.-D. Liao, H. Li, C. Ma, Y. Cui, Y. Shangguan, Z. Huang, Y. Qi, W. Li, Z. Y. Meng, J. Wen, and W. Yu, *Nat. Commun.* **11**, 5631 (2020).